sensors

MDPI

Article

Enhancing the Sensing Performance of Zigzag Graphene Nanoribbon to Detect NO, NO_2, and NH_3 Gases

Ehab Salih [1] and Ahmad I. Ayesh [1,2,*]

[1] Department of Mathematics, Statistics and Physics, Qatar University, P.O. Box 2713, Doha, Qatar; e.salih@qu.edu.qa

[2] Center for Sustainable Development, Qatar University, P.O. Box 2713, Doha, Qatar

* Correspondence: ayesh@qu.edu.qa

Received: 23 March 2020; Accepted: 4 April 2020; Published: 15 July 2020

Abstract: In this article, a zigzag graphene nanoribbon (ZGNR)-based sensor was built utilizing the Atomistic ToolKit Virtual NanoLab (ATK-VNL), and used to detect nitric oxide (NO), nitrogen dioxide (NO_2), and ammonia (NH_3). The successful adsorption of these gases on the surface of the ZGNR was investigated using adsorption energy (E_{ads}), adsorption distance (D), charge transfer (ΔQ), density of states (DOS), and band structure. Among the three gases, the ZGNR showed the highest adsorption energy for NO with −0.273 eV, the smallest adsorption distance with 2.88 Å, and the highest charge transfer with −0.104 e. Moreover, the DOS results reflected a significant increase of the density at the Fermi level due to the improvement of ZGNR conductivity as a result of gas adsorption. The surface of ZGNR was then modified with an epoxy group (-O-) once, then with a hydroxyl group (-OH), and finally with both (-O-) and (-OH) groups in order to improve the adsorption capacity of ZGNR. The adsorption parameters of ZGNR were improved significantly after the modification. The highest adsorption energy was found for the case of ZGNR-O-OH-NO_2 with −0.953 eV, while the highest charge transfer was found for the case of ZGNR-OH-NO with −0.146 e. Consequently, ZGNR-OH and ZGNR-O-OH can be considered as promising gas sensors for NO and NO_2, respectively.

Keywords: zigzag graphene nanoribbon; adsorption energy; gas sensor; DOS

1. Introduction

Graphene-based nanomaterials (G-NMs) have been subjected to intensive investigations in recent years due to their remarkable properties and promising application for electronics [1–4]. Nevertheless, it has been reported that graphene has some limitations in its sensing properties to some kinds of gas molecules such as CO, CO_2, CH_4, N_2, NO_2, NH_3, and H_2, affecting its usage for applications in the field of gas sensors [5–8]. These limitations can be solved either by functionalizing the surface of graphene or generating a G-NM which exhibits a tunable band gap that is referred to as a graphene nanoribbon (GNR) [9,10]. GNRs can be produced either by etching or patterning graphene along a specific direction [11–13]. In addition, practical challenges are still to be resolved in order to utilize graphene for practical sensors, such as its purity degree, trace metal content, application tests, and practical deposition of graphene-based materials on surfaces [14]. GNRs are considered a promising candidate for the field of gas sensors as compared with other C-NMs, thanks to their long and reactive edges that facilitate the adsorption of gas molecules [15–20]. Furthermore, GNRs have been reported in different forms of devices for utilization as a gas sensor, including field-effect transistors (FETs), chemiresistors, and capacitance sensors, etc. [21,22].

Although there have been great benefits to humans as a result of the continuous developments in technology and industry, there have been serious effects on human health due to the release of hazardous

radiation [23–25] and substances such as toxic gases [26,27] and volatile organic compounds [28,29]. The presence of some of these gases, even at low concentrations, is very dangerous to human life [30]. Monitoring the level of nitrogen-based gases such as NO, NO_2, and NH_3 is of great interest for industry as well as medical applications. For instance, detecting NO molecules in the exhalation process can aid in the diagnosis of some respiratory diseases such as asthma [31,32]. Moreover, one of the main serious effects of NO gas is its easy transformation to the highly toxic NO_2 gas through oxidation [33–36]. NO_2 is a toxic gas which can be produced from diesel engines and combustion of fuel in industry [37]. Consequently, NO_2-based gas sensors are of great importance to humans due to the high toxicity of NO_2. These sensors have been used mainly in detecting pollutants in atmospheric air as well as the detection of explosive vapors [38,39]. On the other hand, monitoring and detecting NH_3 gas molecules is a must in semiconductor and optoelectronic applications as well as for environmental purposes [40,41]. It has been found that annihilation of NH_3 gas molecules at the 50–100 ppm level affects human health negatively through irritation of the throat, nose, and eyes [41,42]. Consequently, monitoring and detecting NO, NO_2, and NH_3 gas molecules are of great importance for overcoming some serious human problems such as air pollution.

Therefore, the main concern of the current study is to improve the adsorption capacity of the zigzag graphene nanoribbon (ZGNR) towards NO, NO_2, and NH_3 gases by functionalizing its surface with epoxy and hydroxyl functional groups (-O- and -OH) to facilitate the adsorption of the gas molecules. Density functional theory (DFT), with the aid of the Atomistic ToolKit Virtual NanoLab (ATK-VNL), has been used to build bare ZGNR and to investigate its capacity to adsorb NO, NO_2, and NH_3 gases. The results reflected good adsorption parameters, indicating the ability of pure ZGNR to detect the three gases. To achieve the goal of this study, three new functionalized ZGNR systems were built: ZGNR-O, ZGNR-OH, and ZGNR-O-OH. The results showed a significant improvement in the adsorption energy, adsorption distance, and charge transfer between the gases and the three modified systems upon surface functionalization.

2. Computational Method

Four different ZGNR systems (bare ZGNR, ZGNR-O, ZGNR-OH, and ZGNR-O-OH) have been investigated by DFT calculations based on the ATK-VNL package in this study. Herein, DFT was utilized to relax and to optimize all atoms and systems until the convergence of force was 0.01 eV/Å. The resulting systems were then used as gas sensors to detect NO, NO_2, and NH_3 gases. The calculations were performed based on the generalized gradient approximation (GGA) of the Perdew–Burke–Ernzerhof (PBE) functional [43,44]. The density mesh cutoff was taken to be 125 Hartree and the force tolerance to be 0.01 eV/Å. Monkhorst–Pack k point sampling of 4 × 2 × 1 was used during all calculations. The successful adsorption of NO, NO_2, NH_3 gases on the surface of ZGNR systems was explored based on the adsorption energy (E_{ads}), adsorption distance (D), charge transfer (ΔQ), band structure, and density of states (DOS). The adsorption energy of the gas molecules on ZGNR systems was calculated using the following formula [45–47]:

$$E_{ads} = E_{ZGNR+gas} - (E_{ZGNR} + E_{gas}) \quad (1)$$

where $E_{ZGNR+gas}$ is the total energy of the optimized structure of any gas molecules adsorbed on any of the different ZGNR systems. E_{ZGNR} is the total energy of each of the ZGNR systems without gas adsorption, and E_{gas} is the total energy of each of the optimized NO, NO_2, and NH_3 gases. Increasing the value of E_{ads} with a negative sign indicates that the adsorption of NO, NO_2, and NH_3 gases on the surface of ZGNR systems is stronger [26,48]. Moreover, the charge transfer between the NO, NO_2, and NH_3 gases and the different ZGNR systems was calculated using Mulliken population analysis [49,50].

3. Results

3.1. ZGNR System

The bare ZGNR system was prepared based on ATK-VNL and investigated as a gas sensor to detect NO, NO_2, and NH_3 gases. The optimized structures of ZGNR before and after adsorption of the three gases are given in Figure 1. The results show that the average C-C bond length of ZGNR is 1.425 Å. The adsorption of NO, NO_2, and NH_3 gases on the surface of ZGNR was explored based on the adsorption energy, adsorption distance, charge transfer, band structure, and DOS. The calculations show that the adsorption energy of NO on ZGNR was −0.273 eV and the adsorption distance was 2.88 Å, as shown in Table 1. Moreover, the Mulliken charge analysis showed −0.104 e transfer between NO and ZGNR during the adsorption process. On the other hand, the adsorption energy, adsorption distance, and charge transfer values between NO_2 and ZGNR were −0.225 eV, 3.11 Å, and 0.040 e, respectively. The positive value of charge transfer in the case of NO_2 gas indicates that the electrons transfer from ZGNR to NO_2. The results also reflect the capability of ZGNR to adsorb NH_3 with −0.091 eV adsorption energy and −0.018 e charge transfer.

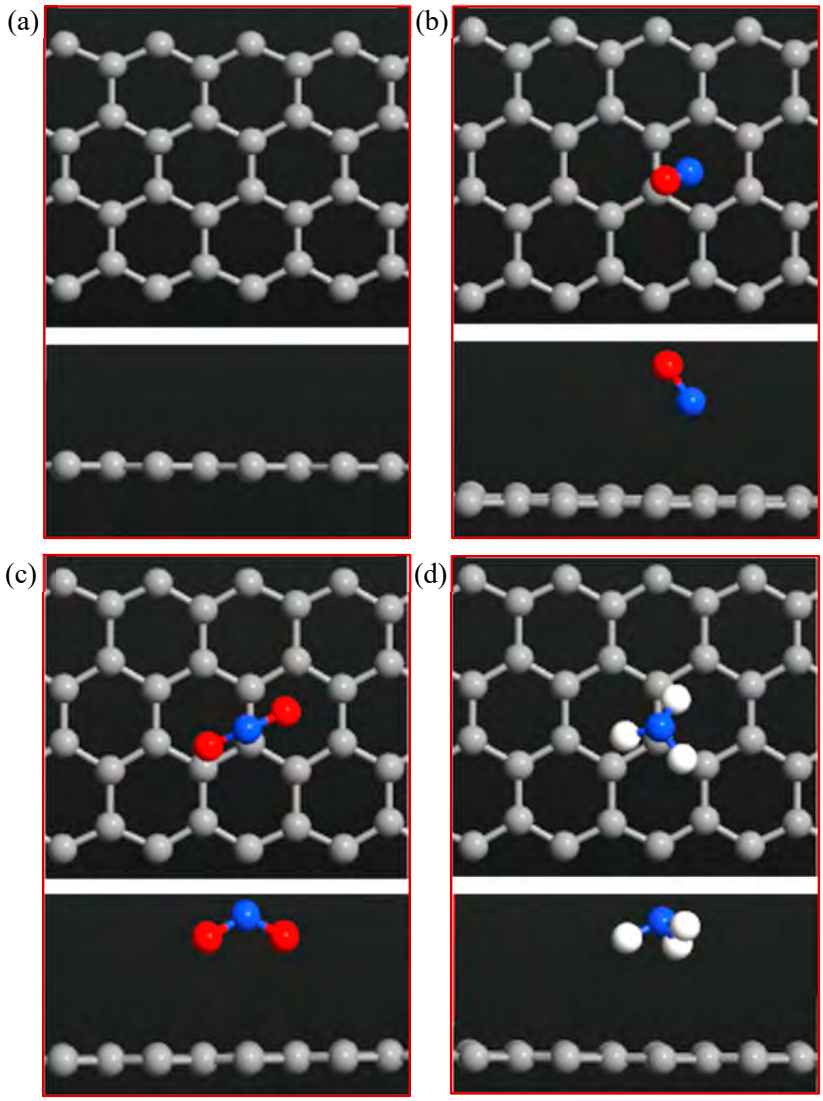

Figure 1. Top and side views of the optimized (**a**) ZGNR, (**b**) ZGNR-NO, (**c**) ZGNR-NO_2, and (**d**) ZGNR-NH_3.

Table 1. Adsorption parameters of the optimized NO, NO_2, and NH_3 gases adsorbed on the zigzag graphene nanoribbon (ZGNR) system. E_{ads}: adsorption energy; D: adsorption distance; ΔQ: charge transfer.

Gas	E_{ads} (eV)	D (Å)	ΔQ (e)
NO	−0.273	2.88	−0.104
NO_2	−0.225	3.11	0.040
NH_3	−0.092	3.03	−0.018

The band structures of ZGNR before and after adsorption of NO, NO_2, and NH_3 gases are shown in Figure 2a–d. The band structure results show that the band gap of ZGNR is 0 eV, reflecting its metallic nature, which has been reported [51,52]. Although no changes in the band gap were observed after the adsorption of NO, NO_2, and NH_3 gases, considerable changes were detected in the DOS results in Figure 3.

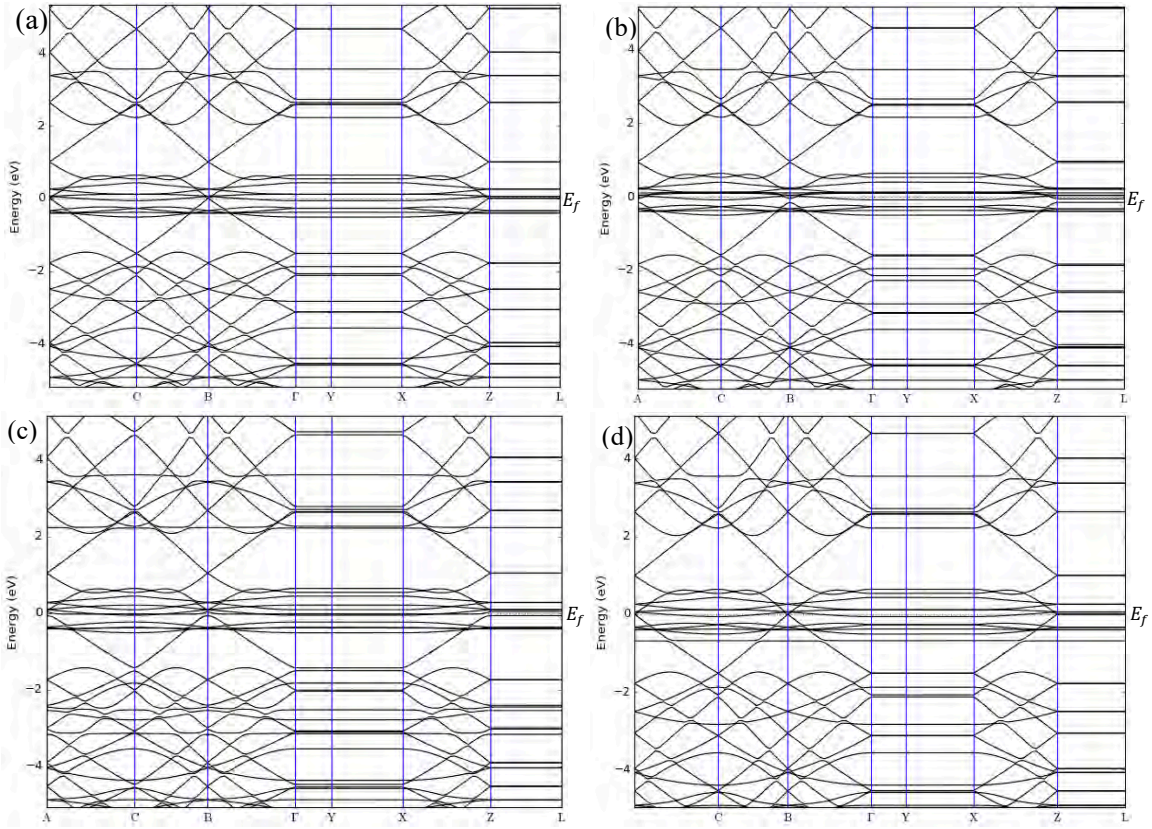

Figure 2. Band structures of (**a**) ZGNR, (**b**) ZGNR-NO, (**c**) ZGNR-NO_2, and (**d**) ZGNR-NH_3.

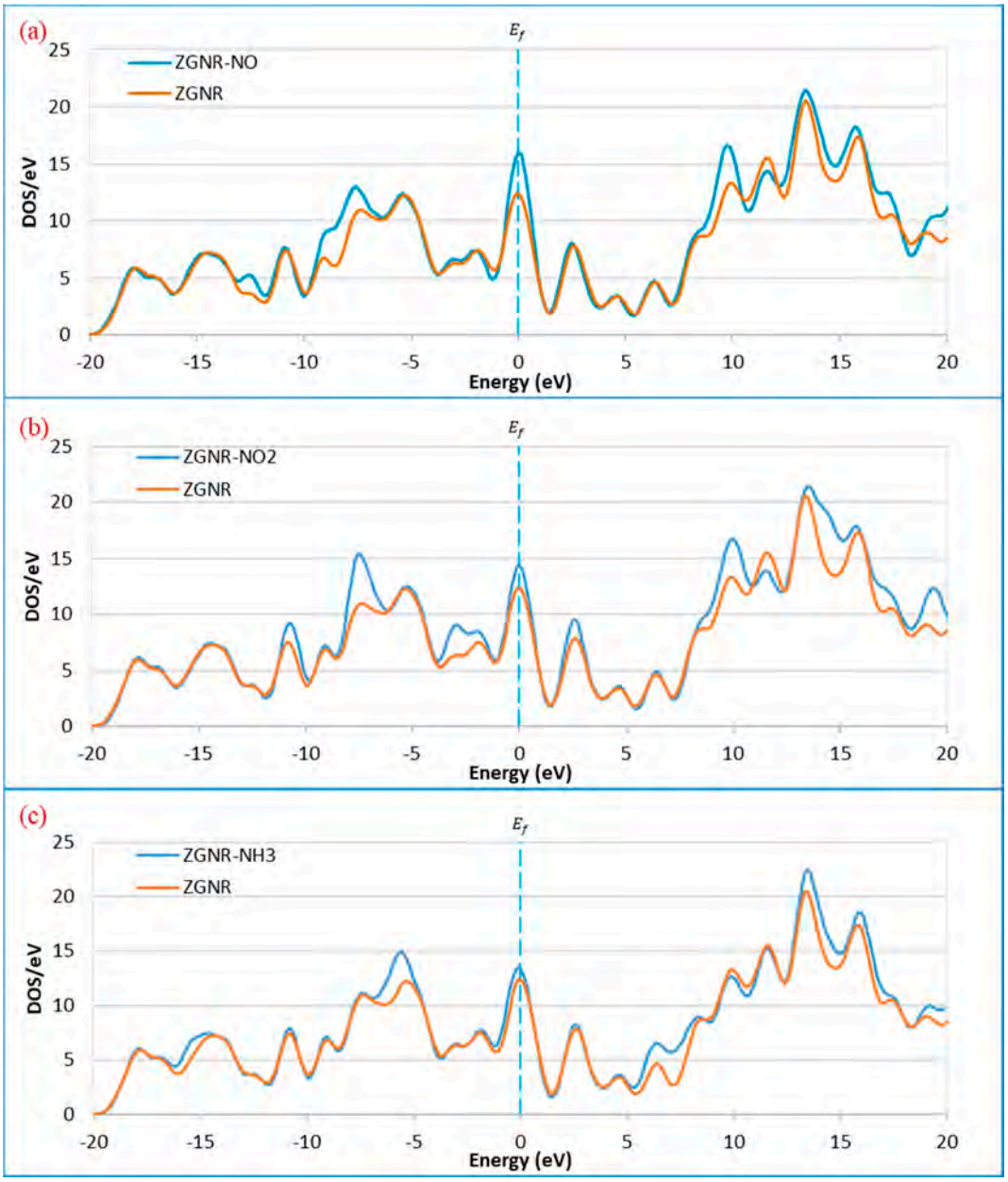

Figure 3. Density of states of the ZGNR system before and after the adsorption of (**a**) NO, (**b**) NO_2, and (**c**) NH_3.

The DOS results show that the DOS at the Fermi level increases significantly after adsorption of NO and NO_2 and slightly for the case of NH_3. In addition to the increase of DOS at the Fermi level, a significant increase was also observed around −12.3, −7.4, 9.9, and 17.3 eV for the case of NO in Figure 3a. For the case of NO_2 in Figure 3b, considerable increases of the DOS around −10.6, −7.4, −2.8, −1.9, 2.8, 9.9, and 19.2 eV were observed after gas adsorption. Meanwhile, increases of DOS for the case of NH_3 were observed around −5.2, 6.5, 13.5, 15.8, and 19.2 eV, as shown in Figure 3c.

3.2. ZGNR-O System

Figure 4a–d shows the optimized structure of the ZGNR-O system before and after adsorption of the gas molecules. The results show that the C-O bond length was 1.39 Å. The adsorption energy, adsorption distance, and charge transfer between the gas molecules and ZGNR-O are shown in Table 2. The adsorption distances between NO, NO_2, and NH_3 gases and ZGNR-O were 2.66, 3.15, and 3.15 Å,

respectively. Although no considerable changes were observed in the adsorption parameters after the adsorption of NO_2 gas, after the functionalization of ZGNR with -O- group, the adsorption energy increased to −0.318 and −0.124 eV for the cases of NO and NH_3. Moreover, the charge transfer between NH_3 gas and ZGNR-O system increased significantly to −0.128 e. Figure 5a–d shows the band structures of ZGNR-O before and after adsorption of NO, NO_2, and NH_3 gases. No significant changes were observed in the band gap after the adsorption of the gas molecules in the band structure results. Nevertheless, a remarkable increase in the DOS at the Fermi level was observed after the adsorption of the three gases on the surface of ZGNR-O, as shown in Figure 6. Figure 6a shows that DOS values around −12.3, −9.0, −7.1, 9.6, 13.5, 16.0, and 22.3 eV increased significantly after adsorption of NO gas. Due to the adsorption of NO_2, a new peak around −21.7 eV was detected, as shown in Figure 6b. In addition, considerable increases were observed around −10.9, −7.1, −2.6, 2.5, 9.6, 13.5, 16.0, 17.5, 18.8, and 22.3 eV, confirming the adsorption of NO_2 gas. For the case of NH_3 in Figure 6c, considerable increases in DOS values around −15.4, −5.2, 6.5, 13.5, 16.0, and 17.5 eV were observed. Moreover, the peaks around 20.8 and 22.4 eV were combined to form a new peak around 21.4 eV.

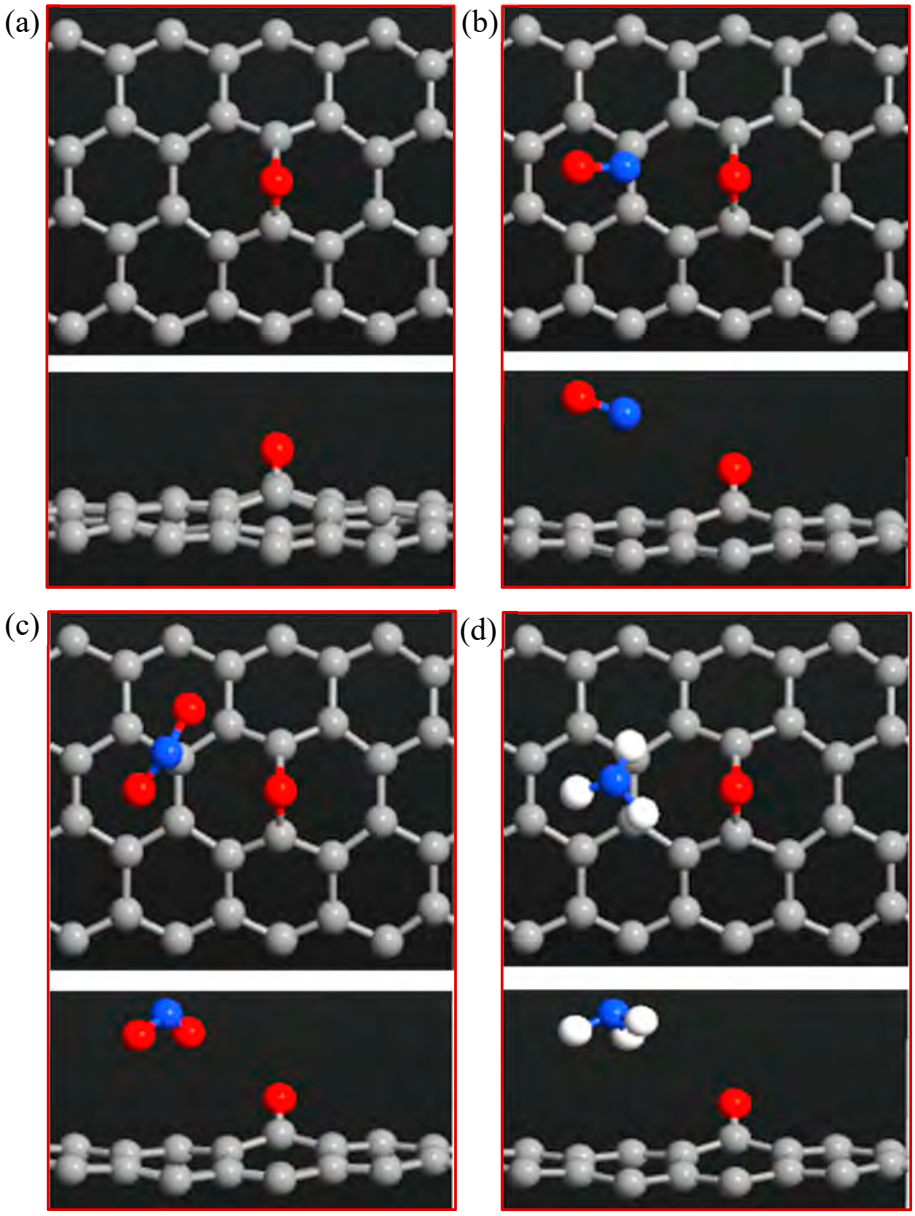

Figure 4. Top and side views of (**a**) ZGNR-O, (**b**) ZGNR-O-NO, (**c**) ZGNR-O-NO_2, and (**d**) ZGNR-O-NH_3.

Table 2. Adsorption parameters of the optimized NO, NO_2, and NH_3 gases adsorbed on the ZGNR-O system.

Gas	E_{ads} (eV)	D (Å)	ΔQ (e)
NO	−0.318	2.66	−0.132
NO_2	−0.212	3.15	0.031
NH_3	−0.124	3.15	−0.128

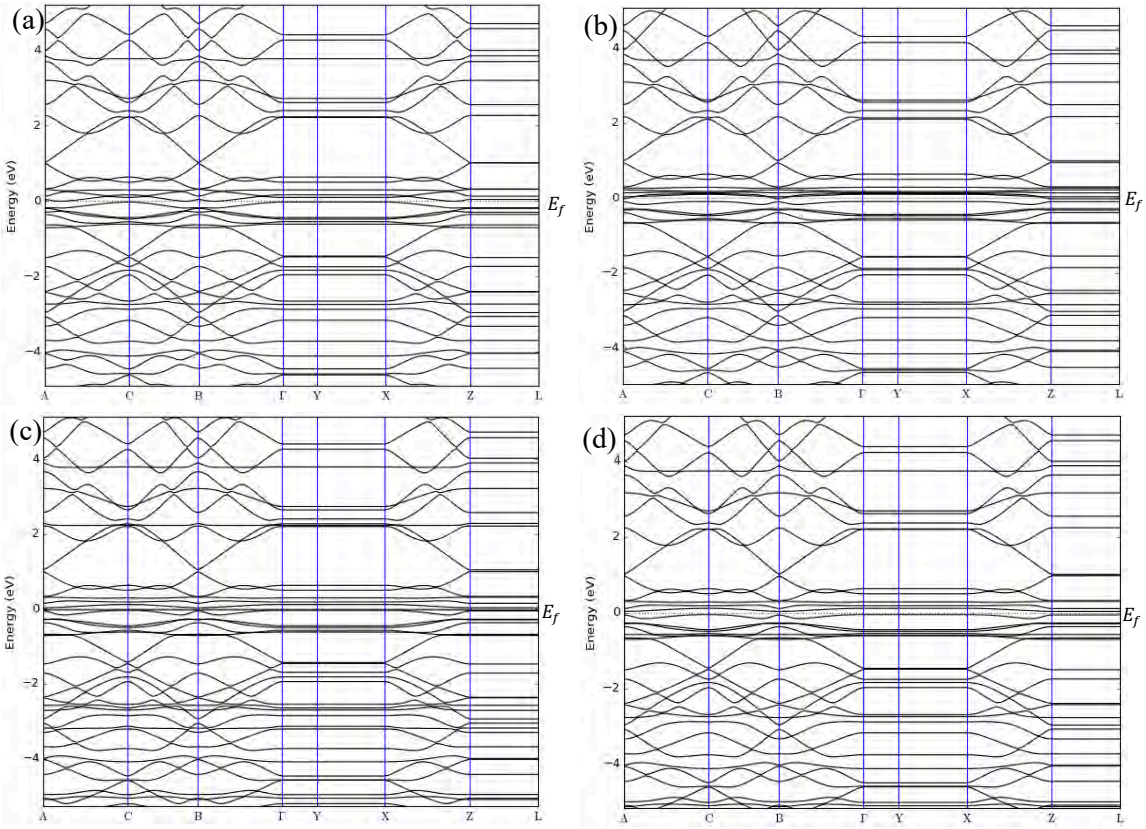

Figure 5. Band structures of (**a**) ZGNR-O, (**b**) ZGNR-O-NO, (**c**) ZGNR-O-NO_2, and (**d**) ZGNR-O-NH_3.

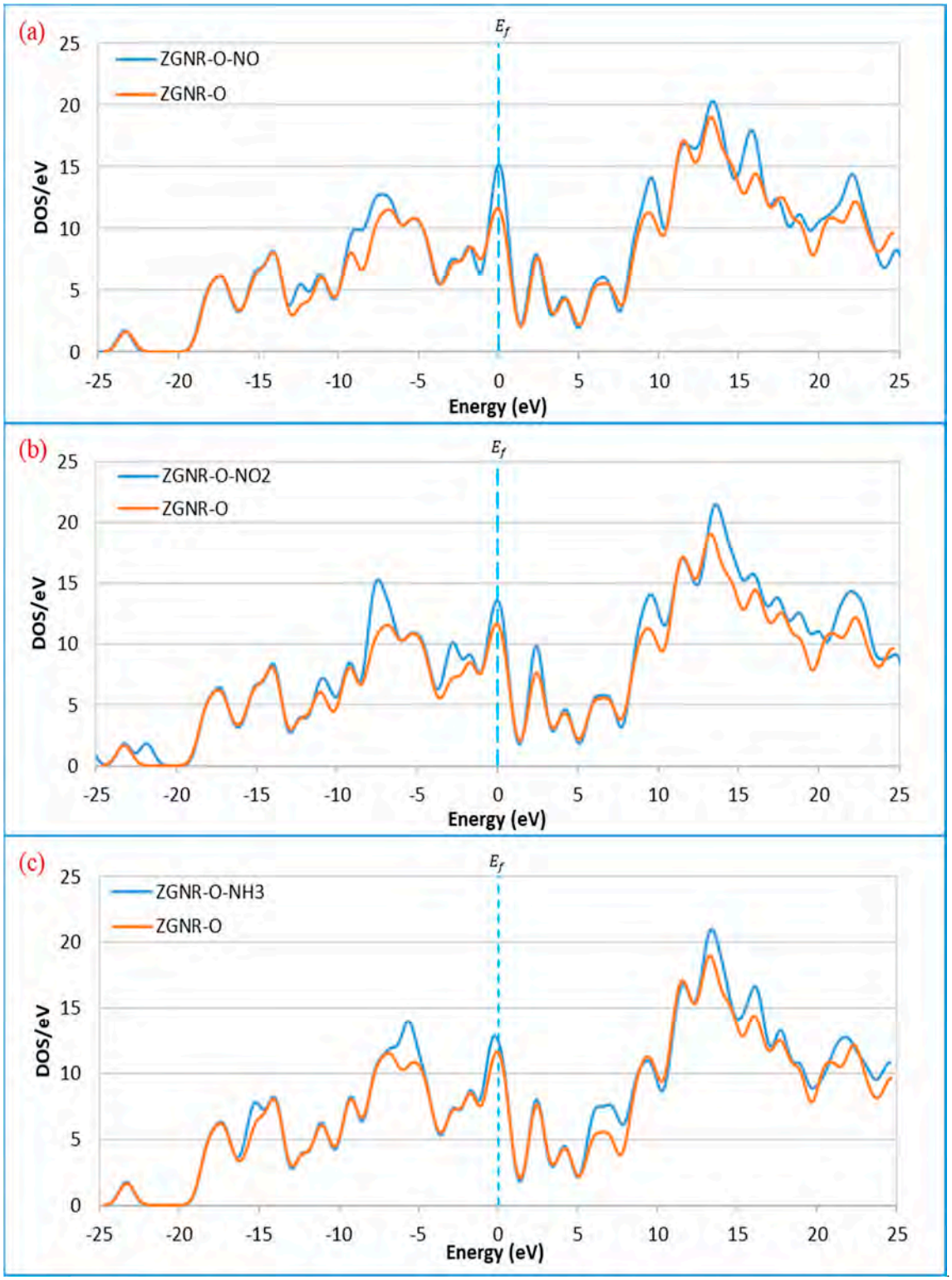

Figure 6. Density of states of the ZGNR-O system before and after the adsorption of (**a**) NO, (**b**) NO_2, and (**c**) NH_3.

3.3. ZGNR-OH System

In this part, the surface of ZGNR was functionalized with one -OH group and then used as a gas sensor to detect NO, NO_2, and NH_3 gases, as shown in Figure 7. The results show that the C-C bond length of ZGNR increased a little to 1.5 Å around the -OH group, while the C-O and O-H bonds

were 1.49 Å and 0.98 Å, respectively. Table 3 shows the adsorption parameters of the optimized NO, NO_2, and NH_3 gases adsorbed on ZGNR-OH. On one hand, the adsorption distances between NO, NO_2, and NH_3 and ZGNR-OH decreased to 2.24, 1.74, and 2.18 Å, respectively. On the other hand, a significant improvement in the adsorption energy was observed with −0.641, −0.618, and −0.244 eV for the cases of NO, NO_2, and NH_3 gases, respectively, as compared with the ZGNR and ZGNR-O systems. Moreover, the Mulliken charge analysis showed that 0.146 and 0.137 e transfer from NO and NH_3 to ZGNR-OH (negative ΔQ) during the adsorption process, while 0.074 e transfer from ZGNR-OH to NO_2. Therefore, the sensing signal is expected to be negative for the former and positive of the latter.

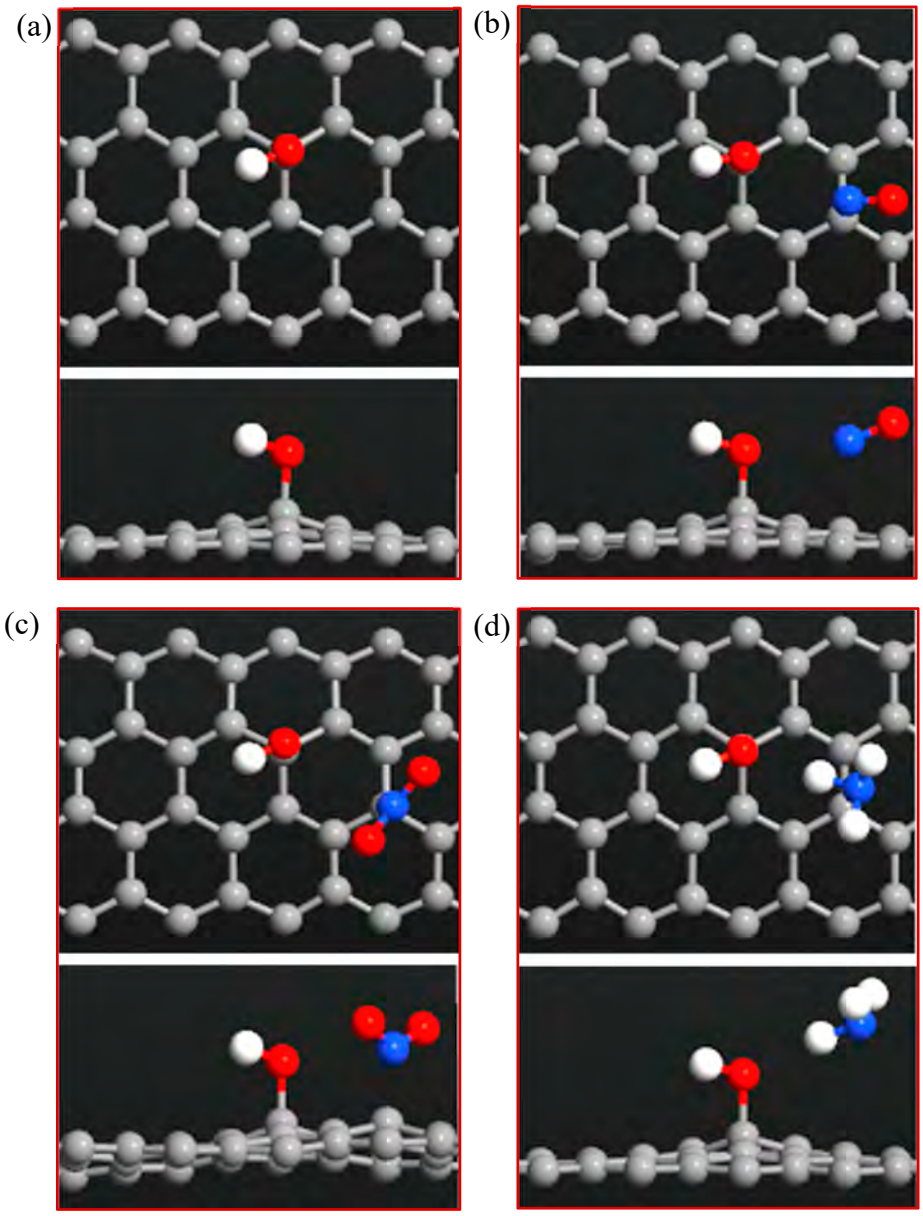

Figure 7. Top and side views of (**a**) ZGNR-OH, (**b**) ZGNR-OH-NO, (**c**) ZGNR-OH-NO_2, and (**d**) ZGNR-OH-NH_3.

Table 3. Adsorption parameters of the optimized NO, NO_2, and NH_3 gases adsorbed on the ZGNR-OH system.

Gas	E_{ads} (eV)	D (Å)	ΔQ (e)
NO	−0.641	2.24	−0.146
NO_2	−0.618	1.74	0.074
NH_3	−0.244	2.18	−0.137

The band structures of ZGNR-OH before and after adsorption of NO, NO_2, and NH_3 gases are shown in Figure 8a–d, respectively. The results show no significant changes in the band gap after the adsorption of NO, NO_2, and NH_3 gases; however, some changes were detected below and above the Fermi level as a result of the gas adsorption.

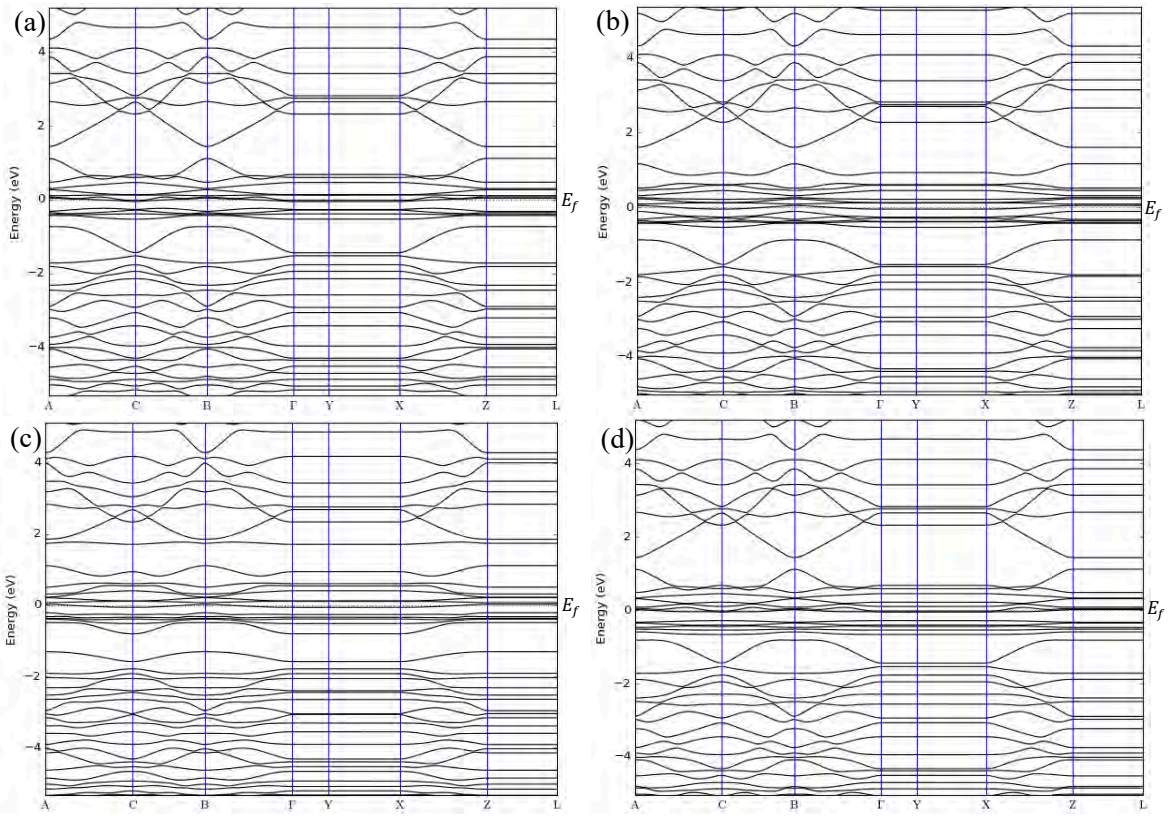

Figure 8. Band structures of (**a**) ZGNR-OH, (**b**) ZGNR-OH-NO, (**c**) ZGNR-OH-NO_2, and (**d**) ZGNR-OH-NH_3.

The DOS results in Figure 9 show that the DOS at the Fermi level increases after the adsorption of NO and NH_3, reflecting an improvement of ZGNR-OH conductivity upon gas adsorption. The results reveal that the DOS around −12.2, −8.9, −7.4, and 9.8 eV increased after the adsorption of NO gas, as shown in Figure 9a, while two new peaks were observed around 21.1 and 22.2 eV. In addition, the peak around 19.9 eV shifted to 19.0 eV. Although no significant change was detected at the Fermi level after the adsorption on NO_2 (Figure 9b), a considerable increase in the DOS around −8.9, −7.4, −2.1, 9.8, and 15.7 eV was detected. Moreover, the peak around −21.0 eV shifted to −21.8 eV, the peak around 19.9 eV shifted to 19.0 eV, and two new peaks around 21.1, and 22.2 eV were observed. Figure 9c shows that the DOS at Femi level increases slightly after the adsorption of NH_3 gas. A significant increase in the DOS around −5.2 and 6.5 eV was also observed.

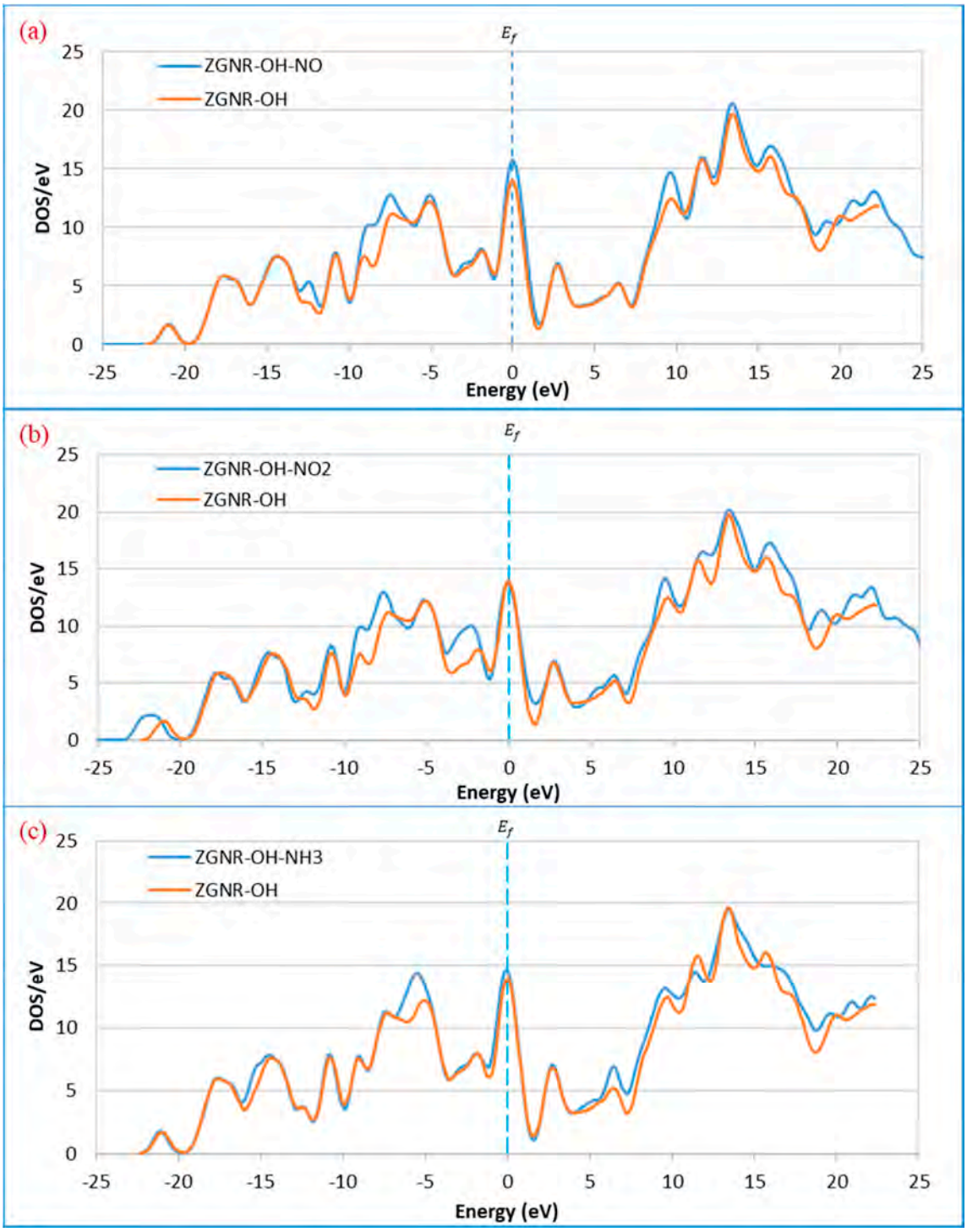

Figure 9. Density of states of the ZGNR-OH system before and after the adsorption of (**a**) NO, (**b**) NO_2, and (**c**) NH_3.

3.4. ZGNR-O-OH System

To improve the adsorption capacity, the surface of ZGNR was functionalized with both -O- and -OH groups, as shown in Figure 10, and then used to detect NO, NO_2, and NH_3 gases. The adsorption energies, adsorption distances, and charge transfer of the optimized NO, NO_2, and NH_3 gases adsorbed on ZGNR-O-OH system are listed in Table 4. The results show that modifying the surface of ZGNR with -O- and -OH groups significantly enhanced its adsorption capacity. For instance, the adsorption

distances decreased to 1.98, 1.68, and 2.45 Å, while the adsorption energies increased significantly to −0.625, −0.953, and −0.219 eV for the cases of the NO, NO_2, and NH_3 gases, respectively. On the other hand, the Mulliken charge analysis demonstrated that 0.118 and 0.141 e transfer from NO and NH_3 to ZGNR-O-OH during the adsorption process, while 0.092 e transfer from ZGNR-O-OH to NO_2 gas.

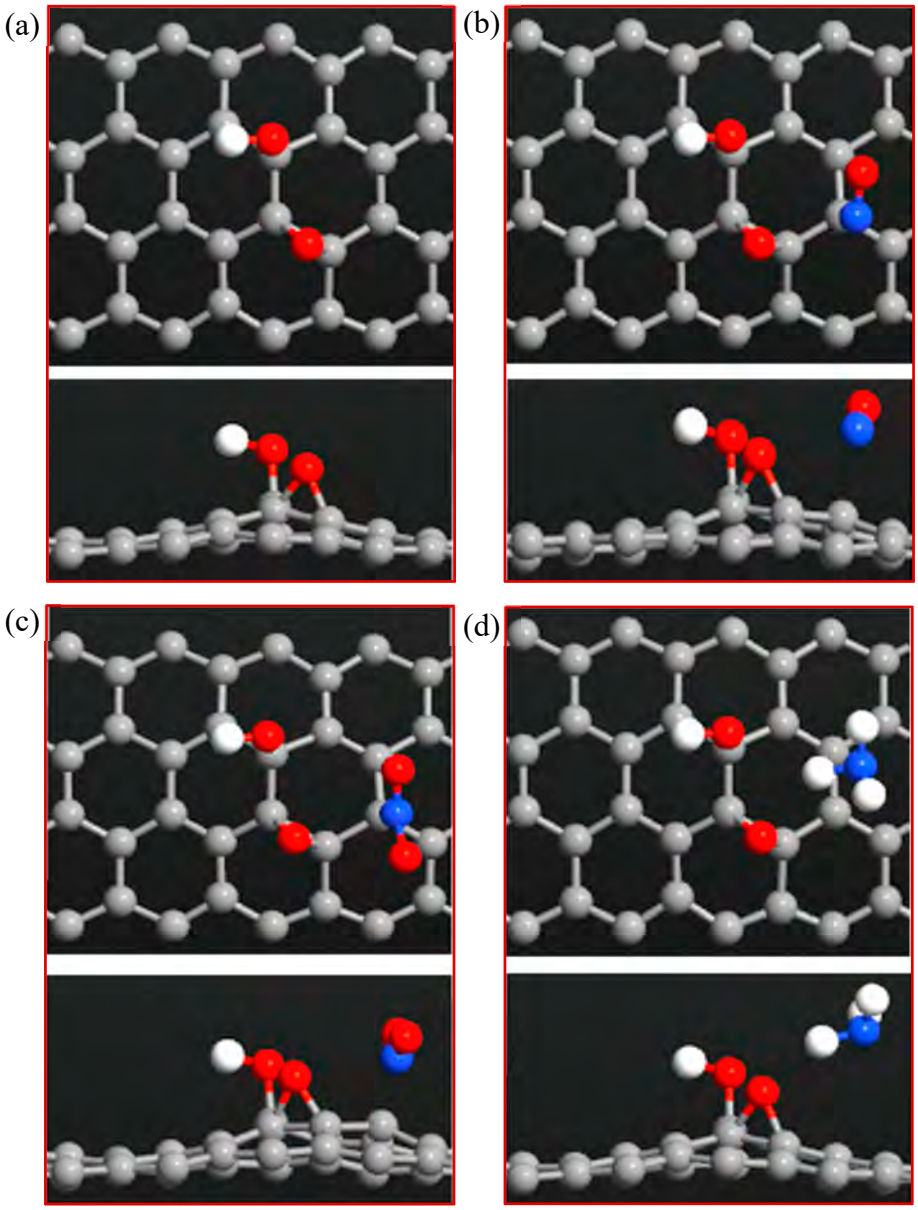

Figure 10. Top and side views of (**a**) ZGNR-O-OH, (**b**) ZGNR-O-OH-NO, (**c**) ZGNR-O-OH-NO_2, and (**d**) ZGNR-O-OH-NH_3.

Table 4. Adsorption parameters of the optimized NO, NO_2, and NH_3 gases adsorbed on the ZGNR-O-OH system.

Gas	E_{ads} (eV)	D (Å)	ΔQ (e)
NO	−0.625	1.98	−0.118
NO_2	−0.953	1.68	0.092
NH_3	−0.219	2.45	−0.141

The band structures of the ZGNR-O-OH system before and after the adsorption of NO, NO_2, and NH_3 gases are shown in Figure 11a–d, respectively. The band structure results show that the band gap of ZGNR increased slightly to 0.043 eV after the functionalization with -O- and -OH groups. The band gap then decreased to 0 eV after the adsorption of the gas molecules, reflecting an improvement in its conductivity and the differentiation between the two cases before and after gas adsorption. Moreover, some other changes were observed below and above the Fermi level due to the adsorption of NO, NO_2, and NH_3 gases.

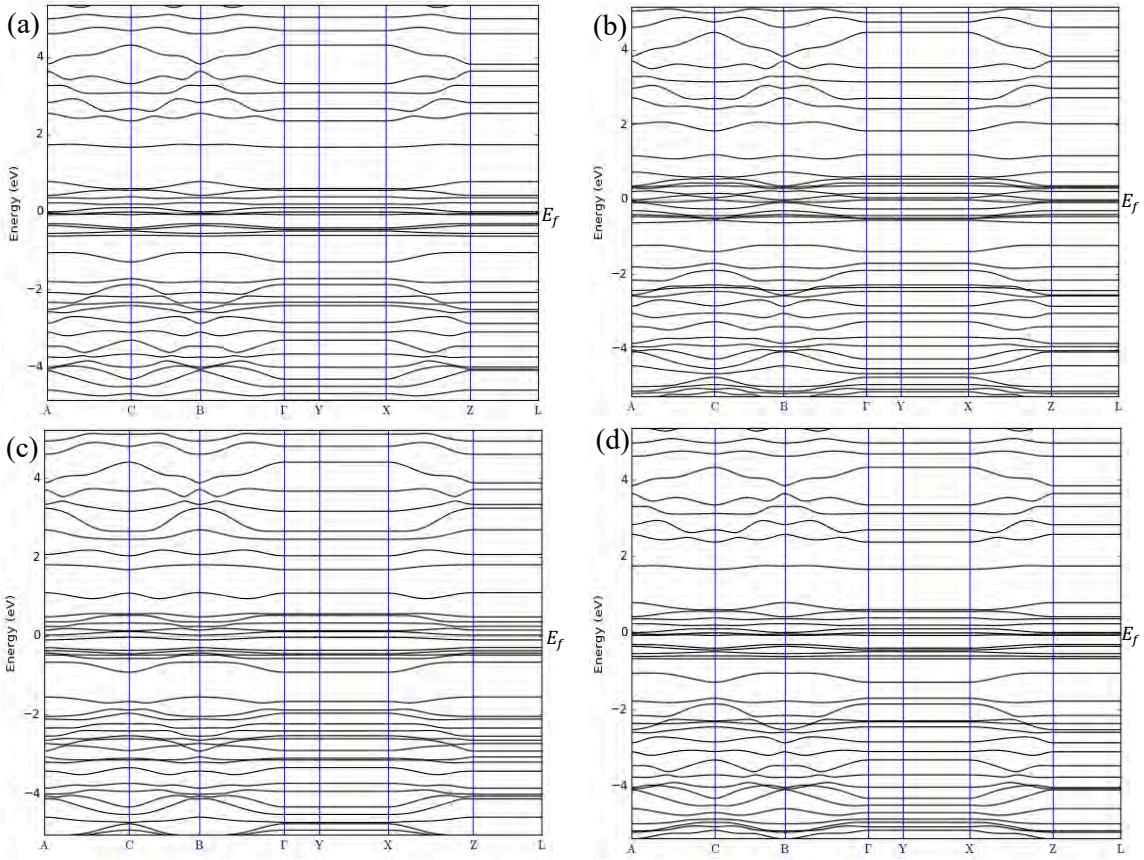

Figure 11. Band structures of (**a**) ZGNR-O-OH, (**b**) ZGNR-O-OH-NO, (**c**) ZGNR-O-OH-NO_2, and (**d**) ZGNR-O-OH-NH_3.

These changes are confirmed by the DOS results in Figure 12. The DOS results show that the DOS at Fermi level increased after the adsorption of NO and NH_3. Figure 12a shows a remarkable increase in the DOS around −12.3, −7.5, 9.6, 13.5, 16.0, and 22.2 eV upon the adsorption of NO gas. The peaks around 18.3 and 19.7 eV shifted to around 17.6 and 18.9 eV and a new peak around 24.3 eV was observed, confirming the adsorption of NO gas on the surface of ZGNR-O-OH. For the case of NO_2 gas in Figure 12b, a significant increase in the DOS around −7.5, −2.5, 16.0, 17.6, and 21.1 eV was detected. Moreover, the peak around −21.0 eV shifted to −21.8 eV and a new peak around 24.0 eV was observed. Figure 12c shows a significant increase in the DOS around −5.2, 6.5, 9.6, 18.2, 19.5, and 22.2 eV after the adsorption of NH_3 gas. In addition, a new peak around 23.7 eV was also observed.

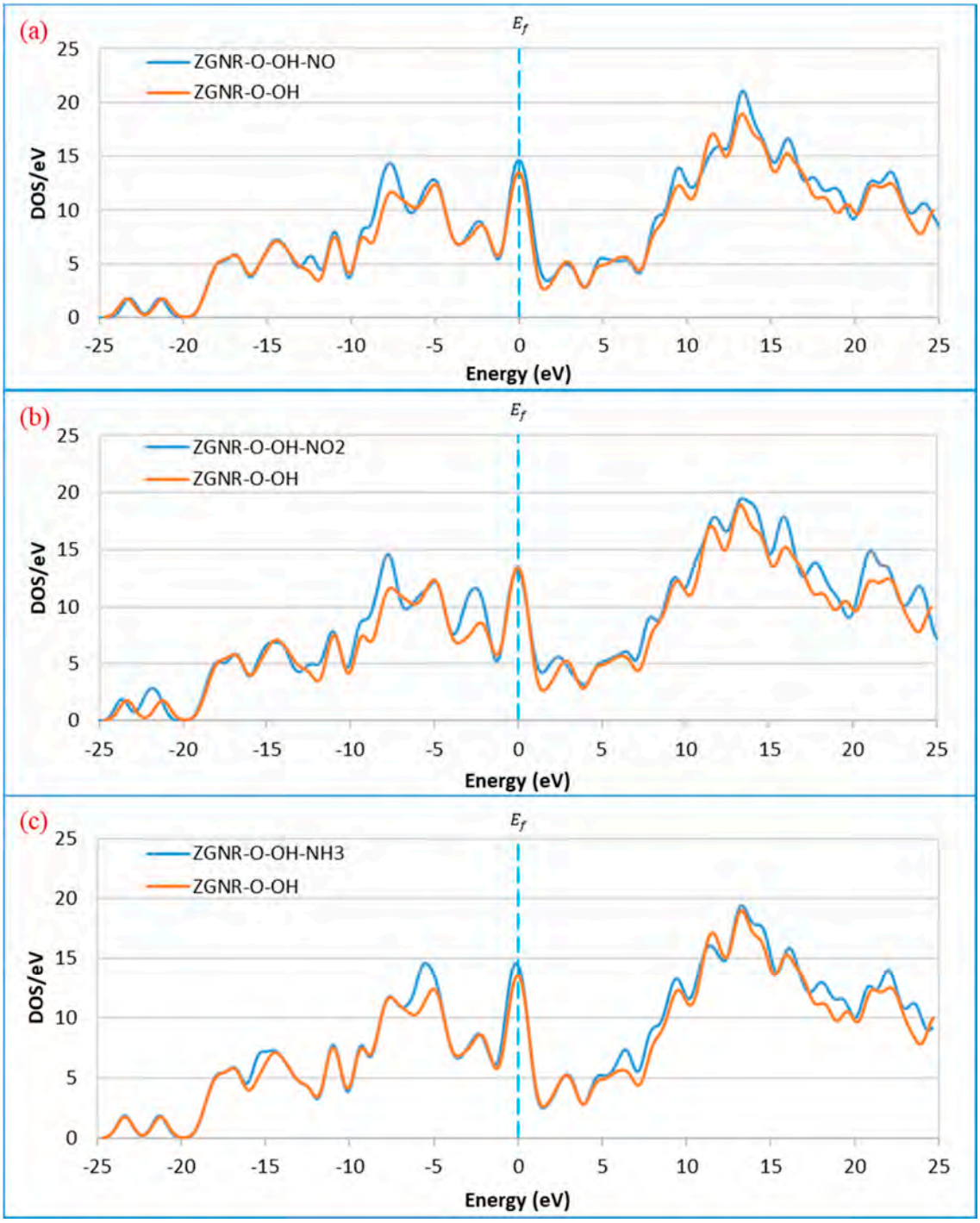

Figure 12. Density of states of the ZGNR-O-OH system before and after the adsorption of (**a**) NO, (**b**) NO_2, and (**c**) NH_3.

4. Discussion

To improve the adsorption capacity of ZGNR, which is goal in this study, the surface of ZGNR was functionalized with -O- and -OH groups, creating three different systems (ZGNR-O, ZGNR-OH, and ZGNR-O-OH). Interestingly, the adsorption parameters of ZGNR reflect a significant improvement upon surface functionalization. This improvement is attributed mainly to the presence of the functional groups, which have been reported to play a significant role in facilitating the adsorption of the gas molecules during the sensing process [53–55].

The Mullekin charge analysis showed that the charge transfer is negative for the cases of NO and NH_3 gases, which is an indication that the charge transfers from the gas molecules to the ZGNR systems (negative sensing signal), which is in good agreement with the reported data stating that NO and NH_3 gases behave as donors [5,56]. On the other hand, for the case of NO_2 the charge transfer was positive, which means that the charge transfers from the ZGNR systems to the gas molecules (positive sensing signal), which have been reported to behave as an acceptor [5,56].

In addition to the adsorption energy, adsorption distance, and charge transfer, the adsorption of NO, NO_2, and NH_3 gases on the surface of the ZGNR systems was also confirmed by the band structure and density of states results. The band structure results show some changes in the bands before and after the Fermi level as a result of the gas adsorption. These changes confirm the successful adsorption of the gas molecules on the surface of ZGNR systems. Moreover, the DOS results demonstrated a significant increase of the density at Fermi level and the appearance of some new peaks. The significant increase in the density of states is related to the improvement of the ZGNR system conductivity upon gas adsorption, which is in good agreement with the reported data that relate the change of adsorbent's conductivity after adsorption of gas molecules [57–59].

The sensing of nitrogen oxides can be assigned to their easy and rapid diffusion on the surface of ZGNR. This leads to formation of hydrogen bonds among the nitrogen oxides and ZGNR, which significantly contributes to increasing their binding energy. The interaction among nitrogen oxides with ZGNR with the epoxy group and hydroxyl groups can be attributed to the development of hydrogen bonds OH ... O(N) between NO_x and -OH and the formation of new weak covalent bonds (C ... N as well as C ... O), as well as H elimination to produce nitrous acid- and nitric acid-like moieties [60,61].

5. Conclusions

The main goal of this study was to enhance the sensing performance of zigzag graphene nanoribbon (ZGNR) towards the detection of NO, NO_2, and NH_3 gases. First, primary calculations using density functional theory (DFT), based on Atomistic ToolKit Virtual NanoLab (ATK-VNL), were used to study the adsorption of the target gases on the surface of the ZGNR. The best sensing performance was found for the case of NO gas, with −0.273 eV adsorption energy and −0.104 e charge transfer during the adsorption process. In order to improve the sensing performance of ZGNR, three different functionalized systems were built: ZGNR-O, ZGNR-OH, and ZGNR-O-OH. The sensing performance towards the three gases was improved significantly after the functionalization, especially for the cases of the ZGNR-OH and ZGNR-O-OH systems. Nevertheless, the best sensing performance from the four systems based on the adsorption energy, adsorption distance, charge transfer, and conductivity improvement was identified for the case of NO gas. Among the four systems, ZGNR-OH with adsorption energy of −0.641 eV and −0.146 e charge transfer was the best. Thus, it is the most selective to NO gas, reflecting that ZGNR-OH can be considered as a promising gas sensor to detect NO gas.

Author Contributions: Conceptualization, A.I.A.; Formal analysis, A.I.A.; Investigation, E.S.; Project administration, A.I.A.; Supervision, A.I.A.; Writing–original draft, E.S.; Writing–review & editing, A.I.A. All authors have read and agreed to the published version of the manuscript.

Acknowledgments: The publication of this article was funded by the Qatar National Library.

Conflicts of Interest: The authors declare no conflict of interest.

References

1. Novoselov, K.; Geim, A.K.; Morozov, S.; Jiang, D.; Zhang, Y.; Dubonos, S.V.; Grigorieva, I.V.; Firsov, A.A. Electric Field Effect in Atomically Thin Carbon Films. *Science* **2004**, *306*, 666–669. [CrossRef] [PubMed]
2. Bolotin, K.I.; Ghahari, F.; Shulman, M.D.; Stormer, H.L.; Kim, P. Observation of the fractional quantum Hall effect in graphene. *Nature* **2009**, *462*, 196–199. [CrossRef] [PubMed]

3. Xia, F.; Mueller, T.; Lin, Y.-M.; Valdes-Garcia, A.; Avouris, P. Ultrafast graphene photodetector. *Nat. Nanotechnol.* **2009**, *4*, 839–843. [CrossRef]
4. Kim, K.S.; Zhao, Y.; Jang, H.; Lee, S.Y.; Kim, J.M.; Kim, K.S.; Ahn, J.-H.; Kim, P.; Choi, J.-Y.; Hong, B.H. Large-scale pattern growth of graphene films for stretchable transparent electrodes. *Nature* **2009**, *457*, 706–710. [CrossRef] [PubMed]
5. Leenaerts, O.; Partoens, B.; Peeters, F.M. Adsorption of H_2O, NH_3, CO, NO_2, and NO on graphene: A first-principles study. *Phys. Rev. B* **2008**, *77*, 125416. [CrossRef]
6. Zhang, Y.-H.; Chen, Y.-B.; Zhou, K.-G.; Liu, C.; Zeng, J.; Zhang, H.-L.; Peng, Y. Improving gas sensing properties of graphene by introducing dopants and defects: A first-principles study. *Nanotechnology* **2009**, *20*, 185504. [CrossRef]
7. Dai, J.; Yuan, J.; Giannozzi, P. Gas adsorption on graphene doped with B, N, Al, and S: A theoretical study. *Appl. Phys. Lett.* **2009**, *95*, 232105. [CrossRef]
8. Robinson, J.T.; Perkins, F.K.; Snow, E.S.; Wei, Z.; Sheehan, P. Reduced Graphene Oxide Molecular Sensors. *Nano Lett.* **2008**, *8*, 3137–3140. [CrossRef]
9. Shao, L.; Chen, G.; Ye, H.; Niu, H.; Wu, Y.; Zhu, Y.; Ding, B. Sulfur dioxide molecule sensors based on zigzag graphene nanoribbons with and without Cr dopant. *Phys. Lett. A* **2014**, *378*, 667–671. [CrossRef]
10. Anasthasiya, A.N.A.; Khaneja, M.; Jeyaprakash, B.G. Electronic Structure Calculations of Ammonia Adsorption on Graphene and Graphene Oxide with Epoxide and Hydroxyl Groups. *J. Electron. Mater.* **2017**, *46*, 5642–5656. [CrossRef]
11. Yang, L.; Cohen, M.L.; Louie, S.G. Magnetic Edge-State Excitons in Zigzag Graphene Nanoribbons. *Phys. Rev. Lett.* **2008**, *101*, 186401. [CrossRef] [PubMed]
12. Zhang, Y.; Tan, Y.-W.; Stormer, H.L.; Kim, P. Experimental observation of the quantum Hall effect and Berry's phase in graphene. *Nature* **2005**, *438*, 201–204. [CrossRef] [PubMed]
13. Han, M.Y.; Özyilmaz, B.; Zhang, Y.; Kim, P.; Oezyilmaz, B. Energy Band-Gap Engineering of Graphene Nanoribbons. *Phys. Rev. Lett.* **2007**, *98*, 206805. [CrossRef] [PubMed]
14. Reina, G.; Gonzalez-Dominguez, J.M.; Criado, A.; Vázquez, E.; Bianco, A.; Prato, M. Promises, facts and challenges for graphene in biomedical applications. *Chem. Soc. Rev.* **2017**, *46*, 4400–4416. [CrossRef]
15. Yan, Q.; Huang, B.; Yu, J.; Zheng, F.; Zang, J.; Wu, J.; Gu, B.-L.; Liu, F.; Duan, W. Intrinsic Current−Voltage Characteristics of Graphene Nanoribbon Transistors and Effect of Edge Doping. *Nano Lett.* **2007**, *7*, 1469–1473. [CrossRef]
16. Huang, B.; Yan, Q.; Zhou, G.; Wu, J.; Gu, B.-L.; Duan, W.; Liu, F. Making a field effect transistor on a single graphene nanoribbon by selective doping. *Appl. Phys. Lett.* **2007**, *91*, 253122. [CrossRef]
17. Cervantes-Sodi, F.; Csányi, G.; Piscanec, S.; Ferrari, A.C. Edge-functionalized and substitutionally doped graphene nanoribbons: Electronic and spin properties. *Phys. Rev. B* **2008**, *77*, 165427. [CrossRef]
18. Zhang, Z.; Liu, B.; Hwang, K.-C.; Gao, H. Surface-adsorption-induced bending behaviors of graphene nanoribbons. *Appl. Phys. Lett.* **2011**, *98*, 121909. [CrossRef]
19. Huang, B.; Li, Z.; Liu, Z.; Zhou, G.; Hao, S.; Wu, J.; Gu, B.-L.; Duan, W. Adsorption of Gas Molecules on Graphene Nanoribbons and Its Implication for Nanoscale Molecule Sensor. *J. Phys. Chem. C* **2008**, *112*, 13442–13446. [CrossRef]
20. Saffarzadeh, A. Modeling of gas adsorption on graphene nanoribbons. *J. Appl. Phys.* **2010**, *107*, 114309. [CrossRef]
21. Fiori, G.; Iannaccone, G. Simulation of Graphene Nanoribbon Field-Effect Transistors. *IEEE Electron Device Lett.* **2007**, *28*, 760–762. [CrossRef]
22. Wang, T.; Huang, D.; Yang, Z.; Xu, S.; He, G.; Li, X.; Hu, N.; Yin, G.; He, D.; Zhang, L. A Review on Graphene-Based Gas/Vapor Sensors with Unique Properties and Potential Applications. *Nano-Micro Lett.* **2015**, *8*, 95–119. [CrossRef] [PubMed]
23. Kim, J.-H.; Mirzaei, A.; Kim, H.W.; Kim, H.; Phan, V.; Kim, S.S. A Novel X-ray Radiation Sensor Based on Networked SnO_2 Nanowires. *Appl. Sci.* **2019**, *9*, 4878. [CrossRef]
24. Al-Sulaiti, L.A.; Salah, B.; Ayesh, A.I. Investigation of flexible polymer-Tl_2O_3 nanocomposites for X-ray detector applications. *Appl. Surf. Sci.* **2019**, *489*, 351–357. [CrossRef]
25. Ayesh, A.I.; Salah, B.; Al-Sulaiti, L.A. Production and characterization of flexible semiconducting polymer-nanoparticle composites for X-ray sensors. *Radiat. Phys. Chem.* **2020**, *167*, 108233. [CrossRef]

26. Aghaei, S.M.; Monshi, M.M.; Calizo, I. A theoretical study of gas adsorption on silicene nanoribbons and its application in a highly sensitive molecule sensor. *RSC Adv.* **2016**, *6*, 94417–94428. [CrossRef]
27. Liu, H.; Zhu, W.; Han, Y.; Yang, Z.; Huang, Y. Single-Nanowire Fuse for Ionization Gas Detection. *Sensors* **2019**, *19*, 4358. [CrossRef]
28. Gancarz, M.; Nawrocka, A.; Rusinek, R. Identification of Volatile Organic Compounds and Their Concentrations Using a Novel Method Analysis of MOS Sensors Signal. *J. Food Sci.* **2019**, *84*, 2077–2085. [CrossRef]
29. Rusinek, R.; Siger, A.; Gawrysiak-Witulska, M.; Rokosik, E.; Malaga-Toboła, U.; Gancarz, M. Application of an electronic nose for determination of pre-pressing treatment of rapeseed based on the analysis of volatile compounds contained in pressed oil. *Int. J. Food Sci. Technol.* **2019**. [CrossRef]
30. Ayesh, A.I.; Alyafei, A.A.; Anjum, R.S.; Mohamed, R.M.; Abuharb, M.B.; Salah, B.; El-Muraikhi, M. Production of sensitive gas sensors using CuO/SnO_2 nanoparticles. *Appl. Phys. A* **2019**, *125*, 550. [CrossRef]
31. Lee, C.-T.; Lee, H.-Y.; Chiu, Y.-S. Performance improvement of nitrogen oxide gas sensors using Au catalytic metal on SnO_2/WO_3 complex nanoparticle sensing layer. *IEEE Sens. J.* **2016**, *16*, 7581–7585. [CrossRef]
32. Di Natale, C.; Paolesse, R.; Martinelli, E.; Capuano, R. Solid-state gas sensors for breath analysis: A review. *Anal. Chim. Acta* **2014**, *824*, 1–17. [CrossRef] [PubMed]
33. Fine, G.F.; Cavanagh, L.M.; Afonja, A.; Binions, R. Metal Oxide Semi-Conductor Gas Sensors in Environmental Monitoring. *Sensors* **2010**, *10*, 5469–5502. [CrossRef] [PubMed]
34. Wetchakun, K.; Samerjai, T.; Tamaekong, N.; Liewhiran, C.; Siriwong, C.; Kruefu, V.; Wisitsoraat, A.; Tuantranont, A.; Phanichphant, S. Semiconducting metal oxides as sensors for environmentally hazardous gases. *Sens. Actuators B Chem.* **2011**, *160*, 580–591. [CrossRef]
35. Marquis, B.T.; Vetelino, J.F. A semiconducting metal oxide sensor array for the detection of NOx and NH_3. *Sens. Actuators B Chem.* **2001**, *77*, 100–110. [CrossRef]
36. Xia, H.; Kong, F.; Wang, S.; Zhu, B.; Guo, X.; Zhang, J.; Wang, Y.; Wu, S. Au-doped WO_3-based sensor for NO_2 detection at low operating temperature. *Sens. Actuators B Chem.* **2008**, *134*, 133–139. [CrossRef]
37. Yang, L.; Marikutsa, A.V.; Rumyantseva, M.; Konstantinova, E.; Khmelevsky, N.; Gaskov, A. Quasi Similar Routes of NO_2 and NO Sensing by Nanocrystalline WO_3: Evidence by In Situ DRIFT Spectroscopy. *Sensors* **2019**, *19*, 3405. [CrossRef] [PubMed]
38. Xia, Y.; Wang, J.; Xu, J.-L.; Li, X.; Xie, D.; Xiang, L.; Komarneni, S. Confined Formation of Ultrathin ZnO Nanorods/Reduced Graphene Oxide Mesoporous Nanocomposites for High-Performance Room-Temperature NO_2 Sensors. *ACS Appl. Mater. Interfaces* **2016**, *8*, 35454–35463. [CrossRef]
39. Jalil, A.R.; Chang, H.; Bandari, V.K.; Robaschik, P.; Zhang, J.; Siles, P.F.; Li, G.; Bürger, D.; Grimm, D.; Liu, X.; et al. Fully Integrated Organic Nanocrystal Diode as High Performance Room Temperature NO_2 Sensor. *Adv. Mater.* **2016**, *28*, 2971–2977. [CrossRef]
40. Kanzawa, K.; Kitano, J. A semiconductor device manufacturer's efforts for controlling and evaluating atmospheric pollution. In Proceedings of the SEMI Advanced Semiconductor Manufacturing Conference and Workshop, Cambridge, MA, USA, 13–15 November 1995; pp. 190–193.
41. Chang, Y.-C.; Bai, H.; Li, S.-N.; Kuo, C.-N. Bromocresol Green/Mesoporous Silica Adsorbent for Ammonia Gas Sensing via an Optical Sensing Instrument. *Sensors* **2011**, *11*, 4060–4072. [CrossRef]
42. Toxicological Profile for Ammonia, U.S. Department of Health and Human Services. Available online: https://www.atsdr.cdc.gov/toxprofiles/tp126.pdf (accessed on September 2004).
43. Perdew, J.P.; Burke, K.; Ernzerhof, M. Generalized Gradient Approximation Made Simple. *Phys. Rev. Lett.* **1996**, *77*, 3865–3868. [CrossRef] [PubMed]
44. Grimme, S. Semiempirical GGA-type density functional constructed with a long-range dispersion correction. *J. Comput. Chem.* **2006**, *27*, 1787–1799. [CrossRef] [PubMed]
45. Gao, W.; Xiao, P.; Henkelman, G.; Liechti, K.; Huang, R. Interfacial adhesion between graphene and silicon dioxide by density functional theory with van der Waals corrections. *J. Phys. D Appl. Phys.* **2014**, *47*, 255301. [CrossRef]
46. Liu, D.; Gui, Y.; Ji, C.; Tang, C.; Zhou, Q.; Li, J.; Zhang, X. Adsorption of SF6 decomposition components over Pd (1 1 1): A density functional theory study. *Appl. Surf. Sci.* **2019**, *465*, 172–179. [CrossRef]
47. Neugebauer, J.; Scheffler, M. Adsorbate-substrate and adsorbate-adsorbate interactions of Na and K adlayers on Al(111). *Phys. Rev. B* **1992**, *46*, 16067–16080. [CrossRef]

48. Manna, B.; Raha, H.; Chakrabarti, I.; Guha, P.K. Selective Reduction of Oxygen Functional Groups to Improve the Response Characteristics of Graphene Oxide-Based Formaldehyde Sensor Device: A First Principle Study. *IEEE Trans. Electron Devices* **2018**, *65*, 1–8. [CrossRef]
49. Bo, Z.; Guo, X.; Wei, X.; Yang, H.; Yan, J.; Cen, K. Density functional theory calculations of NO2 and H2S adsorption on the group 10 transition metal (Ni, Pd and Pt) decorated graphene. *Phys. E Low-Dimens. Syst. Nanostruct.* **2019**, *109*, 156–163. [CrossRef]
50. Mulliken, R.S. Electronic Population Analysis on LCAO–MO Molecular Wave Functions. I. *J. Chem. Phys.* **1955**, *23*, 1833–1840. [CrossRef]
51. Son, Y.-W.; Cohen, M.L.; Louie, S.G. Energy Gaps in Graphene Nanoribbons. *Phys. Rev. Lett.* **2006**, *97*, 216803. [CrossRef]
52. Nakada, K.; Fujita, M.; Dresselhaus, G.; Dresselhaus, M.S. Edge state in graphene ribbons: Nanometer size effect and edge shape dependence. *Phys. Rev. B* **1996**, *54*, 17954–17961. [CrossRef]
53. Toda, K.; Furue, R.; Hayami, S. Recent progress in applications of graphene oxide for gas sensing: A review. *Anal. Chim. Acta* **2015**, *878*, 43–53. [CrossRef]
54. Chatterjee, S.G.; Chatterjee, S.; Ray, A.K.; Chakraborty, A.K. Graphene–metal oxide nanohybrids for toxic gas sensor: A review. *Sens. Actuators B Chem.* **2015**, *221*, 1170–1181. [CrossRef]
55. Peng, Y.; Li, J. Ammonia adsorption on graphene and graphene oxide: A first-principles study. *Front. Environ. Sci. Eng.* **2013**, *7*, 403–411. [CrossRef]
56. Hosseingholipourasl, A.; Ahmadi, M.T.; Ismail, R.; Gharaei, N. Analytical modelling and simulation of gas adsorption effects on graphene nanoribbon electrical properties. *Mol. Simul.* **2017**, *44*, 551–557.
57. Ko, G.; Kim, H.-Y.; Ahn, J.; Park, Y.-M.; Lee, K.-Y.; Kim, J. Graphene-based nitrogen dioxide gas sensors. *Curr. Appl. Phys.* **2010**, *10*, 1002–1004. [CrossRef]
58. Ahmadi, M.T.; Ismail, R.; Anwar, S. *Handbook of Research on Nanoelectronic Sensor Modeling and Applications*; IGI Global: Hershey, PA, USA, 2017.
59. Akbari, E.; Afroozeh, A.; Tan, M.L.P.; Arora, V.K.; Ghadiry, M.; Yusof, R.; Ahmadi, M.T.; Enzevaee, A.; Rahmani, M. Analytical assessment of carbon allotropes for gas sensor applications. *Measurement* **2016**, *92*, 295–302. [CrossRef]
60. Tang, S.; Cao, Z. Adsorption of nitrogen oxides on graphene and graphene oxides: Insights from density functional calculations. *J. Chem. Phys.* **2011**, *134*, 44710. [CrossRef] [PubMed]
61. Guo, L.; Hao, Y.-W.; Li, P.-L.; Song, J.-F.; Yang, R.-Z.; Fu, X.-Y.; Xie, S.-Y.; Zhao, J.; Zhang, W. Improved NO_2 Gas Sensing Properties of Graphene Oxide Reduced by Two-beam-laser Interference. *Sci. Rep.* **2018**, *8*, 4918. [CrossRef] [PubMed]